ROYAL SOCIETY OF CHEMISTRY

PAPER

Check for updates

Synthesis and characterization of thermosetting adhesives from epoxidized *Thevetia peruviana* oil for sustainable bonding solutions

Karthika Vayalachery Kambikanam,[a] Bhadra Purushothaman Bindu,[ac] Adebayo Isaac Olosho ✦*[b] and Kiran Sukumaran Nair ✦*[ac]

The demand for bio-based epoxy thermoset alternatives within the adhesive industry has seen substantial growth in recent years. This increase is attributed to a heightened exploration of renewable materials, including biopolymers and monomers derived from renewable resources. However, despite these significant advancements, a considerable portion of the research primarily focuses on edible oils, which may inadvertently neglect critical implications for food security. So, this study explores the thermal, mechanical, and adhesive properties of epoxy thermosets derived from biobased epoxidized *Thevetia peruviana* oil (ETPO) cured with two diamines, 1,10-decane diamine (DDA) and *m*-xylene diamine (XDA), using imidazole (IM) as a catalytic initiator. The thermosets were evaluated for lap shear strength on stainless steel (SS) and aluminium (Al) substrates at varying imidazole concentrations (0–5%) and curing times (24–96 hours). The results show that DDA-cured thermosets demonstrate superior thermal stability and heat resistance, with $T_{5\%}$ increasing from 149 °C to 256 °C and T_{HRI} from 139 °C to 162 °C as IM concentration rises. XDA-cured thermosets exhibit higher adhesive strength, peaking at 1.47 MPa on SS at 5% IM and 72 hours, but lower thermal stability, with $T_{5\%}$ values decreasing from 157 °C to 68 °C. Imidazole's catalytic efficiency enhanced the crosslinking in both systems, with DDA providing better thermal stability and XDA delivering higher adhesive strength. These findings demonstrate the potential of ETPO-based thermosets as sustainable adhesives, offering excellent performance for industrial applications.

Sustainability spotlight

This study advances sustainable adhesive technology by developing bio-based epoxy thermosets from *Thevetia peruviana* oil (ETPO), a non-edible, renewable feedstock. By replacing petroleum-based adhesives with ETPO-derived thermosets, this research supports SDG 9 (industry, innovation, and infrastructure) through eco-friendly material innovation, SDG 12 (responsible consumption and production) by promoting renewable resources, and SDG 13 (climate action) by reducing reliance on fossil-based materials. Additionally, prioritizing non-edible oils addresses SDG 2 (Zero Hunger) by mitigating competition with food resources. The thermosets exhibit excellent adhesive strength and thermal stability, demonstrating their viability as sustainable bonding solutions for industrial applications. This work aligns with global efforts to transition towards greener, more sustainable material alternatives.

1 Introduction

The quest for eco-friendly polymeric materials has intensified due to environmental concerns and the imperative to reduce reliance on petroleum resources. This has spurred interest in utilizing bio-based binders, such as modified vegetable oils or lignin derivatives, for adhesive synthesis, offering unique structural elements and enhanced adhesion properties. Adhesives play a crucial role in bonding substrates through various mechanisms, influenced largely by their chemical composition and application methods.[1] Epoxy resins, predominant in the thermosetting polymer industry, have attracted attention for their diverse applications, but the environmental and health risks associated with bisphenol A-based compounds necessitate the exploration of sustainable substitutes derived from bio-based precursors, including vegetable oils, lignin, and poly-phenols.[2,3] Recent advancements in adhesive technology have witnessed a shift towards sustainable alternatives, driven by the imperative to mitigate environmental impact and reduce reliance on fossil-based resources. Biobased feedstocks include polyphenol, lignin, vanillin, sorbitol, and vegetable oil.[4] Notably, vegetable oils have emerged as promising candidates for the development of eco-friendly adhesives, offering advantages such as renewability, biodegradability, and low toxicity.

[a]Polymer Science and Engineering, CSIR-National Chemical Laboratory, Pune 411008, India. E-mail: s.kiran@ncl.res.in

[b]Department of Petroleum Chemistry, American University of Nigeria, Yola 640001, Nigeria. E-mail: adebayo.olosho@aun.edu.ng

[c]Academy of Scientific and Innovative Research (AcSIR), Ghaziabad 201002, India

However, the majority of studies in this domain have primarily focused on edible oils, potentially neglecting the broader implications for food security.

In alignment with global sustainability goals, particularly Sustainable Development Goal (SDG) 12 (Responsible Consumption and Production) and SDG 13 (Climate Action), the development of thermosetting adhesives from renewable, non-edible plant oils presents an effective route for reducing greenhouse gas emissions and advancing circular bioeconomy strategies.[5] Biobased polymer systems, such as those derived from vegetable oils, can significantly reduce the carbon footprint associated with adhesive production and use.[6] Moreover, recent studies emphasize the need for credible testing methods and environmental benchmarks to ensure the sustainability claims of biobased products are verifiable and reproducible.[7] Such frameworks support the transition toward certified green materials and facilitate integration into industrial applications.

Zohuriaan-Mehr and colleagues[8] demonstrated the superior adhesion strength of acrylated epoxidized sesame oil (AESSO) and maleated castor oil thermosets compared to traditional bisphenol A-based epoxy resin (DGEBA). This underscores the potential of vegetable oil-derived adhesives as viable alternatives to fossil-based counterparts. Similarly, Chen's group[9] reported the development of fully bio-based pressure-sensitive adhesives (PSAs) incorporating epoxidized soybean oil (ESO) and rosin acid, exhibiting enhanced adhesive properties and compatibility with environmentally friendly materials. In a quest for recyclable adhesives, Li's group[10] formulated epoxy vitrimer adhesives from epoxidized soybean oil (ESO) and dithiol borate ester, offering superior adhesion strength and thermal stability. Moreover, the dynamic borate ester bonds enabled the adhesives' reprocessability and reusability, highlighting their potential for sustainable applications. Boga and coworkers[11] introduced a novel approach to reversible adhesives by combining epoxidized soybean oil (ESO) with coumarins, capable of undergoing reversible cycloaddition reactions under UV irradiation. This design not only demonstrated impressive adhesion strength but also exhibited high reuse efficiency, showcasing its potential for recyclable adhesive systems. Furthermore, Qian and coworkers[12] presented a green strategy for synthesizing a versatile resin from epoxidized soybean oil (ESO) and highly branched polyamine, yielding adhesives with exceptional bonding strength and film-forming ability. The tunable mechanical properties of the resin, coupled with its pressure-sensitive adhesive characteristics, underscore its potential for diverse applications.

Despite these significant advancements, it is evident that much of the research in this field has been concentrated on edible oils, potentially overlooking the implications for food security.[13] Hence, there remains a critical need to explore non-edible oil sources for adhesive synthesis, aligning with the principles of sustainability and resource conservation. *Thevetia peruviana* oil (TPO), obtained from the seeds of *Thevetia peruviana*, stands out as one such resource due to its abundance and potential for versatile utilization. Our prior work established an eco-friendly extraction process for TPO from its seeds,[13] followed by epoxidation, leading to the synthesis of high-performance thermosetting polymers by curing epoxidized TPO (ETPO) with

dicarboxylic acids.[14] This novel approach balances economic feasibility and ecological sustainability, laying the groundwork for TPO's use in protective coatings and reprocessable composite matrices. Expanding on this foundation, the present study focuses on synthesizing and characterizing thermosetting adhesives from ETPO, exploring aliphatic 1,10-diaminodecane (DDA) and *m*-xylene diamine (XDA) as curing agents. We aim to develop adhesive formulations with robust bonding capabilities while prioritizing environmental stewardship. Through comprehensive analysis, we demonstrate the suitability of ETPO-based adhesives for various bonding applications, offering sustainable alternatives in adhesive technology and addressing contemporary challenges in adhesive engineering.

2 Materials

T. peruviana seeds were collected from regions in Pune, India and were extracted and epoxidized to obtained ETPO in accordance to the method stated in our previous studies.[13,15] XDA was obtained from Sigma Aldrich, USA, DDA from TCI Chemicals, Japan, imidazole from Spectrochem PVT Ltd, India and CDCl$_3$ from Meck, USA. All the reagents were used as received unless otherwise specified.

2.1 Methods

2.1.1 Synthesis of ETPO thermoset adhesives. ETPO thermoset adhesives were prepared with an epoxy-amine ratio of 1 : 1 as previously described.[14] First, the imidazole initiator (5 wt%) was dissolved in ETPO at 100 °C with stirring at 500 rpm prior to the addition of the amine hardeners. The curing mixture was applied to an aluminium plate (200 mm^2 area, 60 mg) and cured according to the protocol determined by differential scanning calorimetry (DSC).

2.1.2 Characterization. FTIR analysis was carried out using a Bruker Tensor II FTIR spectrophotometer. To prepare the oil samples, 1 mg of TPO or ETPO was dissolved in 1 mL of chloroform. A background spectrum of chloroform was first recorded before measuring the sample solution using a NaCl window. Infrared spectra of ETPO-TS were obtained in attenuated total reflectance (ATR) mode. For each sample, 32 scans were collected over a wavelength range of 500 to 4000 cm^{-1}. The resulting spectra were processed using Opus 8 software for further analysis.

The reactivity of the curing mixtures was studied using approximately 10 mg of each thermosetting formulation, sealed in a 40 μL TA Hermetic aluminium pan. The samples were heated from room temperature at a rate of 5 °C min^{-1} up to 300 °C across three cycles using a Q10 Differential Scanning Calorimeter (DSC) from TA Instruments, under a constant nitrogen flow of 50 mL min^{-1}. An isothermal curing study was conducted at predetermined temperatures based on the non-isothermal analysis. After the scan, the temperature was quickly reduced to room temperature and ramped at 10 °C min^{-1} to 250 °C for a third cycle to measure residual enthalpy.[16] The degree of cure, α, was estimated using eqn (1)

$$\alpha = \frac{\Delta H_t}{\Delta H_T} \times 100 \quad (1)$$

where ΔH_t is the heat of cure at a given time and ΔH_T is the total heat of reaction during non-isothermal curing. The activation energy of the curing mixtures was calculated using the Ozawa and Kissinger models (eqn (2) and (3), respectively), which relate the heating rates (β) to the peak temperatures (T_p). The kinetics analysis was based on the dependence of heating rates on the peak temperatures, with the activation energy (E_a) and pre-exponential factor (A) determined using the following[17]

$$d(\ln \beta) = -\frac{1.502 E_a}{R} d\left(\frac{1}{T_p}\right) \quad (2)$$

$$d\left(\ln \frac{\beta}{T_p^2}\right) = -\frac{E_a}{R} d\left(\frac{1}{T_p}\right) \quad (3)$$

The thermal stability of the cured thermosets was assessed using a TGA Q5000 analyzer from TA Instruments. Approximately 6.0 mg of each sample was placed in a 100 μL platinum-HT pan and heated from 50 °C to 900 °C at a rate of 10 °C min^{-1} under a nitrogen flow of 25 mL min^{-1}. The heat resistance index (T_{HRI}) of the thermosets was calculated using a formula based on the temperatures where 5% ($T_{5\%}$) and 30% ($T_{30\%}$) weight loss occurred, as per the method described by the authors of ref. 18.

$$T_{HRI} = 0.49 \times \{T_5 + 0.6(T_{30} - T_5)\} \quad (4)$$

The water contact angle (WCA) was determined by using a KRUSS instrument with droplets of Milli-Q water (2 μL). To calculate the mean contact angle values, a minimum of three repeated measurements were taken at various locations on each epoxy surface.

A Universal Testing Machine (UTM) was used to evaluate the thermoset samples. Aluminium and steel plates were prepared, and 50 mg of thermoset adhesive was applied to each plate, covering an area of 200 mm^2. The adhesive was evenly distributed before the plates were joined to ensure proper contact. The adhesive was then cured at 180 °C for 24 to 96 hours. After curing, the bonded area was measured, the specimen was fixed in the UTM, and tension was applied until failure occurred, with the maximum force recorded. Data for each sample were collected in triplicate. The lap shear strength was calculated using eqn (5)

$$\text{Lap shear strength } (N\ mm^{-2}) = \frac{\text{maximum force } (F)}{\text{bonded area } (A)} \quad (5)$$

3 Results and discussion

3.1 Investigation of ETPO-DDA and ETPO-XDA copolymerization by FTIR

ETPO oil was employed in the formulation of a series of thermoset adhesives through the reaction of ETPO with various amines, maintaining a fixed epoxy-to-amine ratio of 1:1. To examine the structural changes associated with the reaction of ETPO with DDA and XDA, in the presence of varying concentrations of imidazole initiator, a comprehensive series of Fourier Transform Infrared (FTIR) analyses was conducted (Fig. 1). The FTIR spectra of ETPO revealed a –C–O oxirane stretching vibration at 826 cm^{-1}, along with characteristic cis –C–C bending at 723 cm^{-1} and –C–O stretching at 1165 cm^{-1}. The spectra also showed methylene and methyl (CH$_3$) bending vibrations at 1461 and 1382 cm^{-1}, respectively, as well as symmetrical and asymmetrical stretching of the methylene group (CH$_2$) at 2926 and 2853 cm^{-1}. Additionally, the carbonyl (–C=O) stretching of the ester appeared at 1743 cm^{-1}. This is similar to what we reported in our previous study.[19] The spectra of the diamines (Fig. 2a) display N–H stretching vibrations at 3751 and 3336 cm^{-1} for DDA, and at 3365 and 3282 cm^{-1} for XDA, which are characteristic of primary amines, consistent with the literature.[20]

The FTIR spectra of the cured thermosets show complete consumption of the epoxy, as indicated by the disappearance of the oxirane peak for both DDA and XDA-cured thermosets at all imidazole concentrations. In contrast, the spectra of thermosets cured without imidazole display residual epoxy peaks,
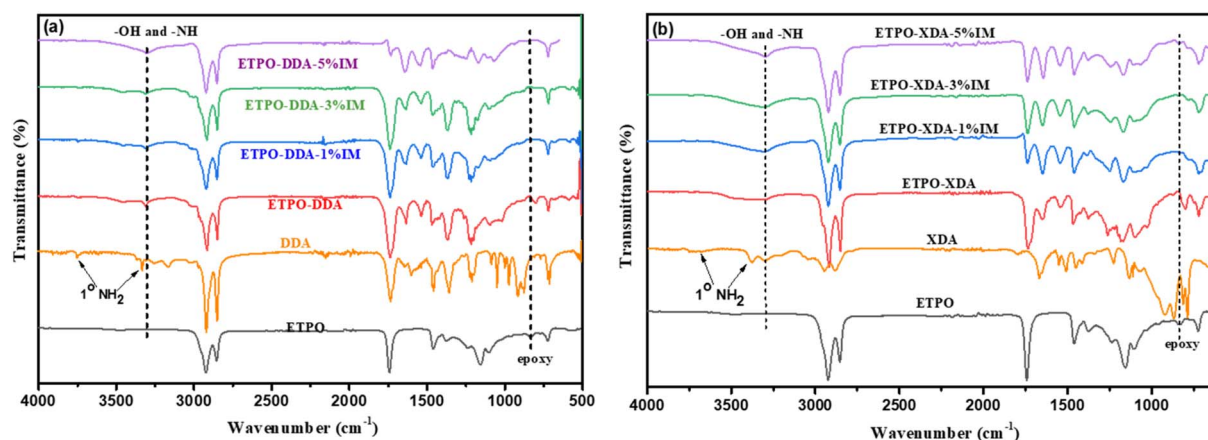

Fig. 1 FTIR spectra of (a) ETPO, DDA, and ETPO-DDA thermosets; (b) ETPO, XDA, and ETPO-XDA thermosets at different IM concentrations.
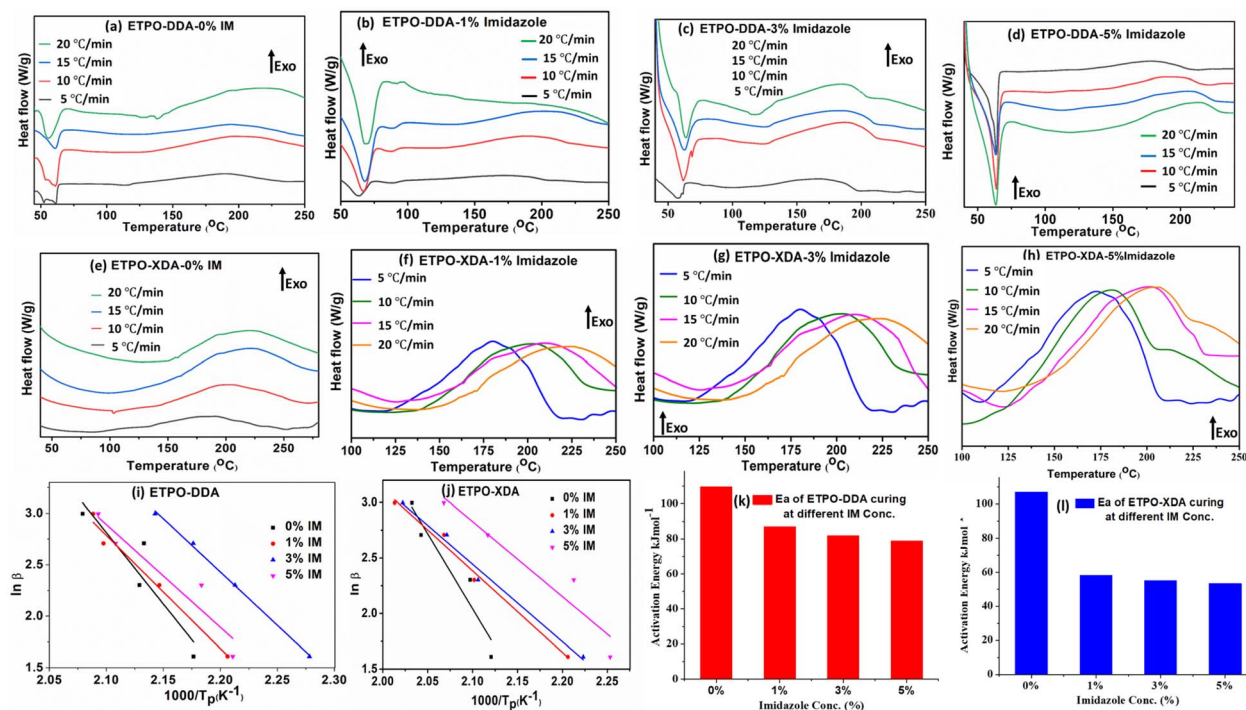
Fig. 2 Thermograms of (a–d) ETPO-DDA and (e–h) ETPO-XDA. Ozawa linear regression for (i) ETPO-DDA and (j) ETPO-XDA. Activation energy at different concentrations of IM for (k) ETPO-DDA and (l) ETPO-XDA.

indicating incomplete curing. The primary amine peaks in DDA and XDA were converted to a single N–H stretching and OH peak at 3301 cm^{-1} in the cured samples, confirming the ring-opening reaction between ETPO and the amines. The N–H and O–H peaks often merge, as noted in previous studies.[21–23] The intensity of this peak increases with higher imidazole concentration, indicating a faster cure rate at higher concentrations of imidazole.

The mechanism by which imidazole functions as an initiator involves two complementary and parallel reaction pathways (Scheme 1). In the primary pathway, imidazole acts as a nucleophile, attacking the epoxy ring to form an imidazolium-alkoxide intermediate. This intermediate can propagate through successive epoxy ring openings via an etherification mechanism, generating a polyether backbone and contributing to crosslink formation. This mechanism has been recently established.[24,25] Concurrently, a second, parallel reaction pathway occurs in which the diamine hardeners directly attack the epoxy rings, resulting in β-hydroxyamine linkages via a classic amine-epoxy addition mechanism (amination). These two pathways, imidazole-initiated etherification and diamine-mediated amination, synergistically contribute to the formation of a densely crosslinked thermoset network.[26] At higher imidazole concentrations, the increased availability of reactive alkoxide species accelerates both pathways, enhancing the overall cure kinetics and network formation. The dual-curing mechanism explains the observed increase in cure extent and mechanical performance with increasing imidazole content. The overall reaction scheme is summarized in Scheme 2.

In particular, the ETPO-derived thermoset adhesives could be considered potentially recyclable because of the presence of ester linkages in their crosslinked structure. These ester linkages, which come from the triglyceride structure of the vegetable oil, are capable of undergoing carboxylate-catalyzed transesterification reactions, which in simpler terms, may rearrange spatially or chemically break down the thermoset matrix, at elevated temperatures or in a basic environment. Studies done in the past on vegetable oil-based vitrimers and on recyclable epoxy systems showed that the bond exchange mechanism of ester networks featuring dynamic covalent bonds provided reprocessability and healability and full dissolution in alkaline media.[27,28] Therefore, the ETPO thermoset system is in accord with the principles of dynamic covalent chemistry, and thus, ester functionality provides opportunities for the design of sustainable and reprocessable bio-based adhesives.

3.2 Differential scanning calorimetric study of ETPO-DDA and ETPO-XDA curing mixtures

The reactivities of curing mixtures consisting of ETPO and two diamines, XDA and DDA, with IM as an initiator, were examined through differential scanning calorimetry (DSC) analysis. The corresponding thermograms at different heating rates and concentrations of the initiator are shown in Fig. 2. The thermogram of the ETPO-DDA mixture exhibits endothermic peaks corresponding to the melting points of DDA, consistent with observations in other studies.[15,29] Conversely, the ETPO-XDA mixture does not display such peaks since XDA's melting point is lower than room temperature. The DSC curves provide
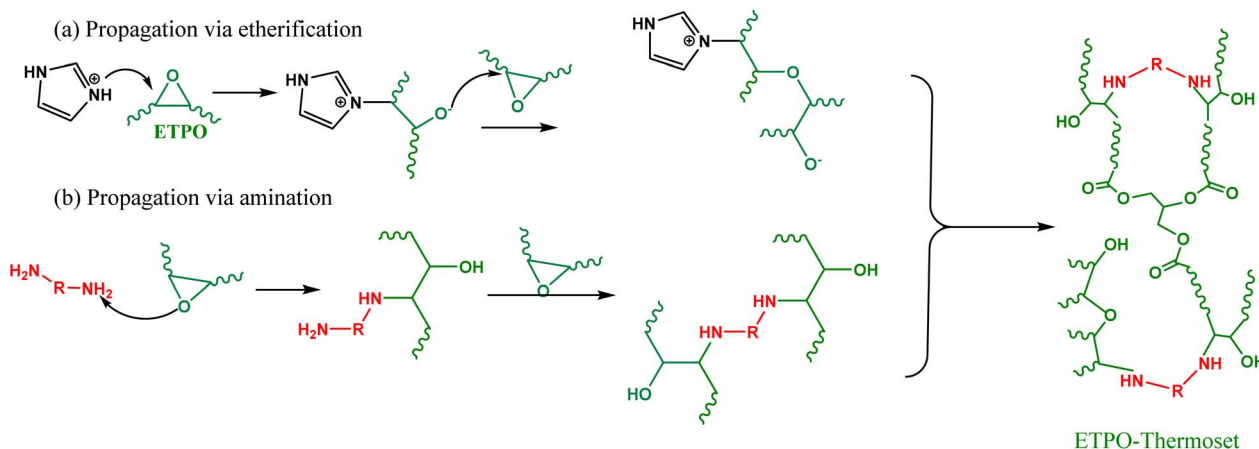
Scheme 1 Possible dual-curing mechanism of ETPO with diamines in the presence of an imidazole initiator, showing parallel (a) etherification (imidazole-initiated) and (b) amination (diamine-initiated) pathways.

critical insights into the onset and progress of ring-opening polymerization (ROP), which is characterized by distinct exothermic peaks indicating the curing reactions of the epoxide rings with the diamines.

For the ETPO-DDA system (Fig. 2a–d) at a heating rate of 5 °C min⁻¹, the uncatalyzed mixture exhibited an onset temperature of 119 °C with a peak exotherm at 192 °C, indicating that the ROP occurs at relatively high temperatures in the absence of a catalyst. Upon introducing 1% IM, the onset dropped to 93 °C, and the peak shifted to 180 °C, suggesting that the imidazole initiates an earlier and more efficient curing process. Further increases in IM concentration continued to reduce the peak temperatures: at 3% IM, onset was 101 °C, peaking at 171 °C, while at 5% IM, onset dropped further to 88 °C, peaking at 162 °C. A similar trend was observed for the ETPO-XDA system (Fig. 2e–h), underscoring the catalytic role of imidazole in promoting earlier ring-opening reactions.

These results clearly demonstrate that the exothermic events in the DSC thermograms correspond to the ROP curing of ETPO

with the diamine hardeners. The reduction in onset and peak temperatures with increasing IM concentration indicates a more efficient initiation mechanism, likely due to enhanced nucleophilic attack on the epoxy groups. Additionally, the distinct differences between catalyzed and uncatalyzed thermograms suggest a shift in the curing pathway upon IM addition, possibly involving different reactive intermediates or propagation steps.

Fig. 2k and l depict the curing activation energy values for ETPO-DDA and ETPO-XDA adhesives, respectively, at varying IM concentrations, estimated using the Ozawa model (Fig. 1i and j). The data reveal that the activation energy for uncatalyzed curing is significantly higher compared to catalyzed curing, underscoring the crucial role of the imidazole catalyst in facilitating the curing process. Moreover, an increase in catalyst concentration further reduces the activation energy in both cases. This reduction is attributed to the higher initiator concentration producing more initiated chains, which leads to a highly selective copolymerization reaction, thus minimizing
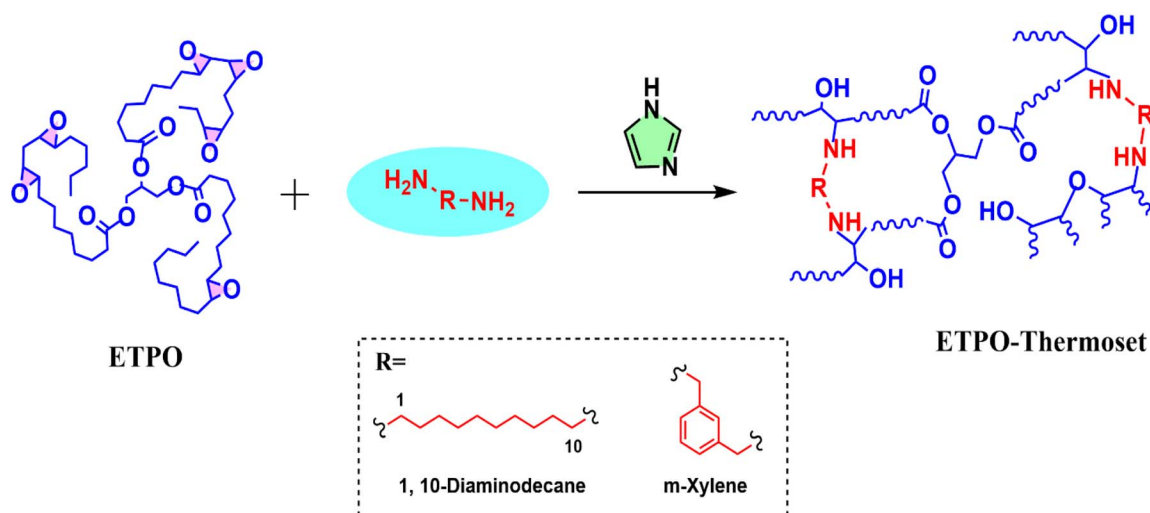
Scheme 2 Possible reaction for the synthesis of the ETPO-amine thermoset.

unwanted reactions and lowering the activation energy.[30] This observed trend aligns with the findings of the Resch-Fauster group[23] during the curing of epoxidized linseed oil. The differences in curing mechanisms between catalyzed and uncatalyzed reactions are also evident in the distinct thermograms (Fig. 2) of these reactions.

The results also indicate that the reactivity of XDA towards ETPO is higher than that of DDA, as evidenced by the lower activation energy of the ETPO-XDA mixture compared to the ETPO-DDA mixture. Several factors contribute to the higher reactivity of epoxy with XDA. XDA's more compact structure, with two amine groups attached to a benzene ring, leads to less steric hindrance during the curing reaction. In contrast, DDA's long, flexible aliphatic chain introduces greater steric hindrance, reducing the accessibility of amine groups for reaction with the epoxy groups.[31] Furthermore, the benzene ring in XDA can delocalize electron density, enhancing the nucleophilicity and reactivity of the amine groups towards the epoxy resin. The aliphatic chain in DDA lacks such electron-donating characteristics, resulting in lower nucleophilicity of the amine groups.[31] The lower activation energy observed in the epoxy-XDA system suggests a lower energy barrier for the curing reaction, possibly due to the structural rigidity of XDA, which promotes a more favorable orientation for the reaction, reducing the energy required for the transition state compared to the more flexible DDA.[32]

This study builds on and extends recent investigations into the reactivity of bio-based epoxidized oils with multifunctional curing agents. For instance, Mija's[33] and Chen's groups[34] have demonstrated that the curing of epoxidized linseed oil and soybeans with dicarboxylic acids is strongly dependent on the concentration and type of imidazole initiator used, where increased initiator levels reduced the activation energy significantly, similar to the current findings with ETPO-XDA and ETPO-DDA systems. Similarly, Kumar *et al.*[35] reported the imidazole-catalyzed curing of epoxidized soybean oil (ESO) with anhydrides, emphasizing the catalytic influence on curing kinetics and crosslink density. However, the current study distinguishes itself by comparing aliphatic and aromatic diamines as curing agents in the presence of imidazole, a rarely explored combination in epoxidized oil thermoset research. Notably, while other studies often use anhydrides or carboxylic acids, this work investigates primary amines, enabling deeper insight into the influence of backbone rigidity and steric effects on curing behavior and adhesive properties. The lower activation energy and enhanced reactivity of the XDA system compared to DDA offers a new direction for optimizing both kinetics and network architecture in biobased epoxy adhesives.

3.3 Thermal behaviour of ETPO thermosets

The thermal properties of ETPO thermosets were assessed using thermogravimetric analysis (TGA), with the results summarized in Table 1 and thermograms shown in Fig. 3. TGA data, including temperatures at 5% and 30% decomposition ($T_{5\%}$ and $T_{30\%}$) and the heat resistance index (T_{HRI}), highlight the impact of varying imidazole (IM) concentrations on the thermal

Table 1 $T_{5\%}$, $T_{30\%}$ and T_{HRI} for ETPO thermosets determined by TGA analysis

ETPO thermosets	$T_{5\%}$ (°C)	$T_{30\%}$ (°C)	T_{HRI} (°C)
ETPO-DDA-1%IM	149	374	139
ETPO-DDA-3%IM	155	379	142
ETPO-DDA-5%IM	256	382	162
ETPO-XDA-1%IM	157	367	139
ETPO-XDA-3%IM	97	376	130
ETPO-XDA-5%IM	68	358	119

stability of the thermosets. Higher imidazole concentrations significantly improve the thermal stability of DDA-cured thermosets. $T_{5\%}$ increased from 149 °C at 1% IM to 256 °C at 5% IM, while $T_{30\%}$ rose from 374 °C to 382 °C. This increase reflects more extensive crosslinking, which enhances thermal resistance, consistent with previous studies on vegetable oil-based thermosets.[36] T_{HRI} values also rose from 139 °C to 162 °C, indicating improved heat resistance with increasing IM concentrations. However, XDA-cured thermosets exhibit a different trend. While $T_{30\%}$ remains relatively stable (358 °C to 376 °C), $T_{5\%}$ decreases from 157 °C at 1% IM to 68 °C at 5% IM, suggesting premature decomposition at higher IM concentrations. This reduction is likely due to less efficient crosslinking in XDA systems, where the rigid aromatic structure may hinder uniform network formation, leading to localized weaknesses and early degradation.[37,38] T_{HRI} values also decrease from 139 °C to 119 °C, indicating a potential destabilizing effect of excessive imidazole on XDA-cured thermosets.

These results suggest that DDA's flexible aliphatic structure promotes better crosslinking and thermal stability, while XDA's rigidity leads to complex degradation pathways, including the breakdown of aromatic structures.[38] Imidazole's efficiency as a catalyst varies with the curing agent, impacting crosslinking density and overall thermal properties.[39–42]

3.4 Adhesive strength and wetting behaviour of cured ETPO thermosets

The lap shear strength of ETPO thermosets cured with XDA and DDA was evaluated on aluminium (Al) and stainless steel (SS) substrates at varying IM concentrations and curing times. The results, illustrated in Fig. 4, reveal several key trends in adhesion performance. For both XDA and DDA, the lap shear strength increased with curing time, peaking at 72 hours. Beyond this point, the strength either plateaued or slightly decreased, suggesting an optimal curing time of 72 hours for maximum adhesive performance. At 0% IM, the lap shear strength of DDA on Al increased from 0.0014 MPa at 24 hours to 0.35 MPa at 96 hours, and on SS from 0.015 MPa to 0.43 MPa. With 1% IM, the strength peaked at 0.222 MPa on Al and 0.266 MPa on SS at 72 hours. At 3% IM, the maximum strength reached 0.43 MPa on Al and 0.53 MPa on SS at 72 hours. The highest strength with DDA was observed at 5% IM, reaching 0.788 MPa on Al and 1.11 MPa on SS at 72 hours.

For XDA, the lap shear strength on Al increased from 0.013 MPa at 24 hours to 0.41 MPa at 96 hours, and on SS from
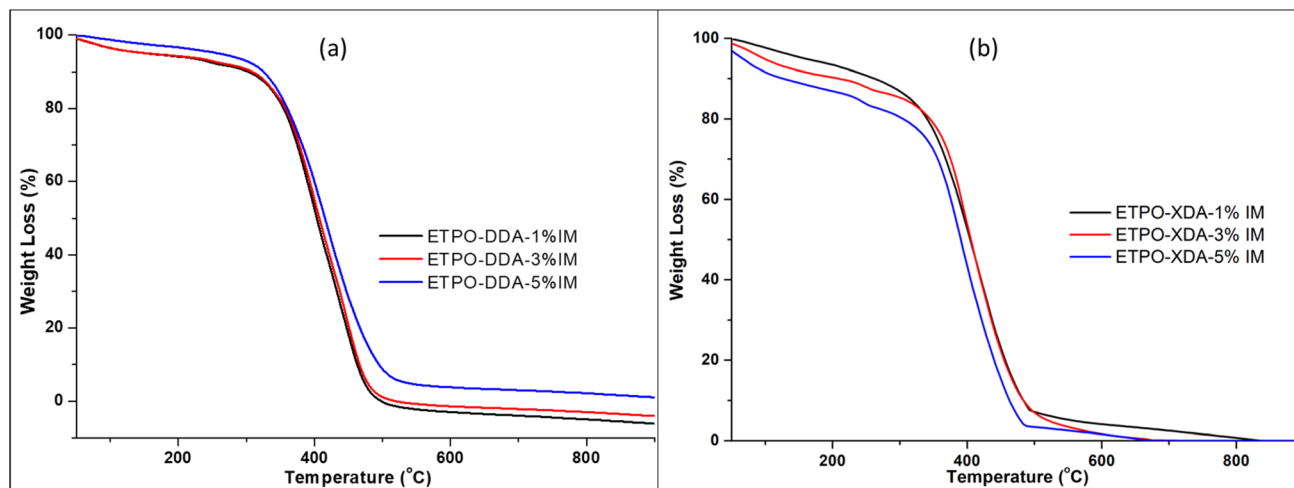
Fig. 3 TGA thermograms of the (a) ETPO-DDA and (b) ETPO-XDA adhesives at different IM conc.

0.028 MPa to 0.59 MPa at 0% IM. At 1% IM, the strength peaked at 0.34 MPa on Al and 0.384 MPa on SS at 72 hours. At 3% IM, the maximum strength reached 0.6 MPa on Al and 0.68 MPa on SS at 72 hours. The highest strength with XDA was recorded at 5% IM, with 0.952 MPa on Al and 1.47 MPa on SS at 72 hours. XDA consistently showed higher lap shear strength compared to DDA across all imidazole concentrations, indicating that XDA may facilitate a higher crosslinking density within the ETPO matrix. The loss of strength with XDA beyond 72 hours is probably caused by over-curing effects. XDA, as an aromatic and stiff component, creates a highly crosslinked network early in the curing process. Sustained thermal exposure beyond the optimal point of crosslinking might trigger internal stress buildup, embrittlement, and microvoid formation at the adhesive-substrate interface, resulting in diminished lap shear performance.[43] Furthermore, excess post-curing can cause interfacial adhesion degradation because of hindered mobility of network chains and potential oxidative or thermal degradation in localized areas.[44] Conversely, the aliphatic and flexible nature of DDA allows for slower and more gradual crosslinking with the ability of the thermoset to withstand extended curing times without mechanical degradation.

Adhesive strength was always greater on stainless steel (SS) than on aluminium (Al). One may attribute this difference to differences in surface chemistry and surface energy. Stainless steel is normally present with chromium, which helps to form a passive oxide layer with increased surface reactivity.[45] Although we did not carry out surface analysis to verify the precise surface composition, it is documented that these oxide layers are capable of supporting secondary interactions (e.g., hydrogen bonding or polar interactions) with polar functional groups like epoxides.[46] In contrast, Al forms a stable oxide layer that is less reactive, hindering strong bond formation with the adhesive.[47,48]

The contact angle measurements further clarify the observed adhesion trends (Fig. 4e). ETPO-DDA-5%IM exhibited a contact angle of $110.4 \pm 0.33°$, while ETPO-XDA-5%IM recorded a slightly higher value of $113.08 \pm 0.33°$. These values indicate relatively hydrophobic adhesive surfaces with limited wetting on both substrates.[49] The marginally higher contact angle for ETPO-XDA suggests reduced spreading and interfacial interaction, which may partially explain the observed decline in lap shear strength of XDA systems upon prolonged curing despite their higher initial crosslink density. Thus, while XDA confers higher cohesive strength to the adhesive matrix, its lower wettability compared to DDA may restrict optimal interfacial adhesion, particularly at extended curing times when embrittlement becomes more pronounced.

The adhesion strength increased with curing time and IM concentration, peaking at 72 hours and 5% IM concentration, respectively. Longer curing times allow for more extensive crosslinking within the thermoset matrix, enhancing the cohesive strength of the adhesive.[50] Higher imidazole concentrations accelerate the curing reaction, leading to a more densely crosslinked network, which translates to higher adhesion strength.[51] Imidazole, as a nucleophilic catalyst, improves the nucleophilicity of the amine hardeners, facilitating the ring-opening polymerization of epoxy groups. This results in a more efficient curing process, particularly at higher imidazole concentrations, where the formation of imidazolium intermediates accelerates the reaction.[30]

These results align with previous studies on vegetable oil-based epoxy adhesives.[11,52–55] Zhang et al.[56] obtained a shear strength of 1.7 MPa from isophthalic acid-functionalized soybean oil, while Del Prado et al.[57] achieved 1.5 MPa using plant oil-acrylate epoxy latex from palm, rubber seed, and *Sapium sebiferum* oil. Most of these studies used edible vegetable oil without consideration for sustainability in terms of food security.

To evaluate short-term durability, selected formulations were immersed in water for 24 h and tested for lap shear strength (Fig. 4f). Post-immersion values were 0.712 MPa (ETPO-DDA-5%IM/Al), 0.731 MPa (ETPO-DDA-5%IM/SS), 1.0087 MPa (ETPO-XDA-5%IM/Al), and 1.1778 MPa (ETPO-
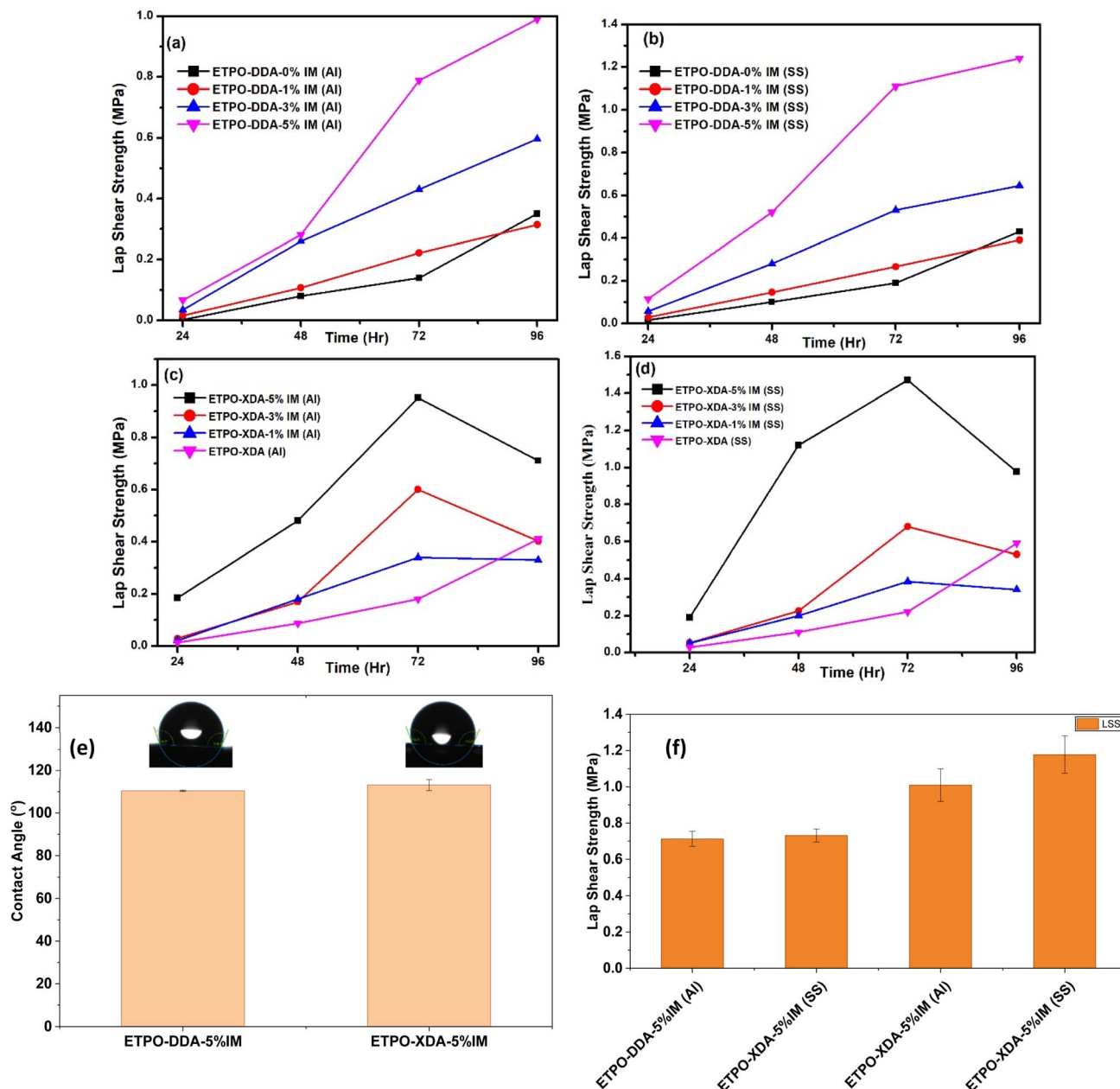
Fig. 4 Lap shear strength of (a) ETPO-DDA adhesives on aluminium sheets; (b) ETPO-DDA adhesives on stainless sheets; (c) ETPO-XDA adhesives on aluminium sheets; and (d) ETPO-XDA adhesives on aluminium sheets cured at different IM concentration and time; (e) LSS under water for 24 h; (f) contact angle of ETPO-DDA-5%IM and ETPO-XDA-5%IM.

XDA-5%IM/SS), corresponding to strength retentions of ~90%, ~66%, ~100%, and ~80% of their dry values, respectively. The XDA-based systems maintained the highest absolute and relative strengths, reflecting their higher crosslink density and greater hydrophobicity, which reduced water ingress and hydrolytic degradation. In contrast, the larger loss observed for DDA on SS indicates greater interfacial vulnerability to water-induced debonding.

4 Conclusion

This study highlights the versatility of epoxy thermosets derived from epoxidized *Thevetia peruviana* oil (ETPO) as bio-based

adhesives for industrial applications. The results demonstrate that DDA-cured thermosets exhibit superior thermal stability, with higher $T_5\%$, $T_{30}\%$, and T_{HRI} values, making them ideal for high-temperature environments. On the other hand, XDA-cured thermosets provide higher adhesive strength, especially on stainless steel substrates, but are more prone to premature degradation. The influence of imidazole as a catalyst significantly enhances crosslinking, leading to improved mechanical and thermal properties in both DDA and XDA systems. The optimal performance in adhesive strength was observed at 5% IM concentration and 72 hours curing time, suggesting a balance between catalyst efficiency and crosslink density. These findings demonstrate the potential of ETPO-based

thermosets as sustainable alternatives to conventional petrochemical-based adhesives, contributing to the development of eco-friendly materials with promising thermal and mechanical properties for various industrial applications. Importantly, this work aligns with global sustainability frameworks, particularly the United Nations Sustainable Development Goals (SDGs).

Conflicts of interest

There are no conflicts to declare.

Data availability

All data relevant to this study have been presented in this manuscript.

References

1 L. A. Heinrich, *Green Chem.*, 2019, **21**, 1866–1888.

2 P. Verdugo, D. Santiago, S. De la Flor and À. Serra, *ACS Sustain. Chem. Eng.*, 2024, **12**, 5965–5978.

3 A. I. Olosho, F. Amoo Adekola, K. S. Nair, A. V. Ambade, T. O. Uthman, O. D. Saliu, A. A. Adeleke, M. Onuoha, A. O. Abdulsamad and M. A. Yuguda, in *2023 2nd International Conference on Multidisciplinary Engineering and Applied Science (ICMEAS)*, IEEE, 2023, pp. 1–6.

4 A. I. Olosho, F. Amoo Adekola, K. S. Nair, A. V. Ambade, T. O. Uthman, O. D. Saliu, A. A. Adeleke, M. Onuoha, A. O. Abdulsamad and M. A. Yuguda, in *2023 2nd International Conference on Multidisciplinary Engineering and Applied Science (ICMEAS)*, IEEE, 2023, pp. 1–6.

5 Ż. Ciastowicz, R. Pamuła and A. Białowiec, *Materials*, 2024, **17**, 1738.

6 L. A. Heinrich, *Green Chem.*, 2019, **21**, 1866–1888.

7 J. Thomas, R. S. Patil, M. Patil and J. John, *Coatings*, 2024, **14**, 774.

8 Z. Karami, M. J. Zohuriaan-Mehr, K. Kabiri and N. Ghasemi Rad, *Polym. Renewable Resour.*, 2019, **10**, 27–44.

9 Y.-F. Lei, X.-L. Wang, B.-W. Liu, X.-M. Ding, L. Chen and Y.-Z. Wang, *ACS Sustain. Chem. Eng.*, 2020, **8**, 13261–13270.

10 C. Li, Y. Chen, Y. Zeng, Y. Wu, W. Liu and R. Qiu, *Eur. Polym. J.*, 2022, **162**, 110923.

11 K. Boga, A. F. Patti, J. C. Warner, G. P. Simon and K. Saito, *ACS Appl. Polym. Mater.*, 2023, **5**, 4644–4653.

12 Z. Qian, S. Liu, G. Du, S. Wang, Y. Shen, X. Zhou, S. Jiang, H. Niu, Z. Duan and T. Li, *ACS Sustain. Chem. Eng.*, 2023, **11**, 5315–5324.

13 A. I. Olosho, S. K. Nair, A. V. Ambade and F. A. Adekola, *ACS Agric. Sci. Technol.*, 2023, **3**, 1014–1024.

14 A. I. Olosho, M. S. Alam, K. Sukumaran Nair, A. V. Ambade and F. A. Adekola, *ACS Appl. Polym. Mater.*, 2024, **26**, 590–591.

15 A. I. Olosho, M. S. Alam, K. S. Nair, A. V. Ambade and F. A. Adekola, *ACS Appl. Polym. Mater.*, 2024, **6**(5), 2695–2708.

16 G. Gerami, R. Bagheri and R. Darvishi, *J. Therm. Anal. Calorim.*, 2019, **137**, 575–582.

17 J. J. P. Barros, I. D. D. S. Silva, N. G. Jaques and R. M. R. Wellen, *J. Mater. Res. Technol.*, 2020, **9**, 13539–13554.

18 M. R. M. Hafiezal, A. Khalina, Z. A. Zurina, M. D. M. Azaman and Z. M. Hanafee, *J. Compos. Sci.*, 2019, **3**, 6.

19 A. I. Olosho, M. S. Alam, K. Sukumaran Nair, A. V. Ambade and F. A. Adekola, *ACS Appl. Polym. Mater.*, 2024, **26**, 590–591.

20 R. Ahmadi and A. Ullah, *ACS Sustain. Chem. Eng.*, 2020, **8**, 8049–8058.

21 Z. Baig, N. Akram, K. M. Zia, M. Saeed, M. K. Khosa, L. Ali and S. Saleem, *J. Appl. Polym. Sci.*, 2020, **137**, 1–9.

22 H. Zhao, S. Xu, A. Guo, J. Li and D. Liu, *Thermochim. Acta*, 2021, **702**, 178987.

23 A. Todorovic, K. Resch-Fauster, A. R. Mahendran, G. Oreski and W. Kern, *J. Appl. Polym. Sci.*, 2021, **138**, 1–13.

24 J. Herzberger, K. Niederer, H. Pohlit, J. Seiwert, M. Worm, F. R. Wurm and H. Frey, *Chem. Rev.*, 2016, **116**, 2170–2243.

25 T. N. Tran, C. Di Mauro, A. Graillot and A. Mija, *Polym. Chem.*, 2020, **11**, 5088–5097.

26 M. Wang, Z. Zhang and W. Zhang, *Acc. Chem. Res.*, 2022, **55**, 2708–2727.

27 C. Di Mauro, T. N. Tran, A. Graillot and A. Mija, *ACS Sustain. Chem. Eng.*, 2020, **8**, 7690–7700.

28 R. Dinu, U. Lafont, O. Damiano and A. Mija, *Ind. Crops Prod.*, 2024, **222**, 119645.

29 C. Ding, G. Tian and A. Matharu, *Mater. Today Commun.*, 2016, **7**, 51–58.

30 T. N. Tran, C. Di Mauro, A. Graillot and A. Mija, *Macromolecules*, 2020, **53**, 2526–2538.

31 J. Wan, C. Li, Z.-Y. Bu, C.-J. Xu, B.-G. Li and H. Fan, *Chem. Eng. J.*, 2012, **188**, 160–172.

32 F. Fraga and E. Rodriguez Nunez, *J. Appl. Polym. Sci.*, 2001, **80**, 776–782.

33 T. N. Tran, C. Di Mauro, A. Graillot and A. Mija, *Macromolecules*, 2020, **53**, 2526–2538.

34 X. M. Ding, L. Chen, D. M. Guo, B. W. Liu, X. Luo, Y. F. Lei, H. Y. Zhong and Y. Z. Wang, *ACS Sustain. Chem. Eng.*, 2021, **9**, 3267–3277.

35 S. Kumar, S. K. Samal, S. Mohanty and S. K. Nayak, *Ind. Eng. Chem. Res.*, 2017, **56**, 687–698.

36 Q. Tang, J. Jiang, J. Li, L. Zhao and Z. Xi, *Polymers*, 2024, **16**, 1229.

37 R. Teijido, L. Ruiz-Rubio, S. Lanceros-Méndez, Q. Zhang and J. L. Vilas-Vilela, *Polymers*, 2023, **15**(20), 4180.

38 C. Di Mauro, A. Genua and A. Mija, *Polymers*, 2021, **13**, 2503.

39 Y. Xue, C. Li, J. Tan, Z. Su, Y. Yang, G. Zhang and Q. Zhang, *J. Mater. Sci.*, 2020, **55**, 7321–7336.

40 B. Yang, Y. Mao, Y. Zhang, G. Bian, L. Zhang, Y. Wei, Q. Jiang, Y. Qiu and W. Liu, *Polymer*, 2019, **178**, 121586.

41 M. S. Fedoseev, L. F. Derzhavinskaya, I. A. Borisova and T. E. Oshchepkova, *Russ. J. Appl. Chem.*, 2022, **95**, 357–365.

42 K. Leena, P. B. Soumyamol, M. Baby, S. Suraj, R. Rajeev and D. S. Mohan, *J. Therm. Anal. Calorim.*, 2017, **130**, 1053–1061.

43 T. Guo, J. He, X. Pang, A. A. Volinsky, Y. Su and L. Qiao, *Acta Mater.*, 2017, **138**, 1–9.

44 X. Han, Y. Jin, W. Zhang, W. Hou and Y. Yu, *J. Adhes. Sci. Technol.*, 2018, **32**, 1643–1657.

45 C. Örnek, B. Payam, A. Gloskovskii, K. Kazmanlı, N. Mohamed, B. Derin, M. Ürgen, C.-E. Chou, H.-W. Yen, B. Avcı and S. Ooi, *npj Mater. Degrad.*, 2023, **7**, 71.

46 Y. Kotb, A. Cagnard, K. R. Houston, S. A. Khan, L. C. Hsiao and O. D. Velev, *J. Colloid Interface Sci.*, 2022, **608**, 634–643.

47 T. H. Wu, A. Foyet, A. Kodentsov, L. G. J. van der Ven, R. A. T. M. van Benthem and G. de With, *Mater. Chem. Phys.*, 2014, **145**, 342–349.

48 S. Maulana, E. S. Wibowo, E. Mardawati, A. H. Iswanto, A. Papadopoulos and M. A. R. Lubis, *Polymers*, 2024, **16**, 1613.

49 G. H. Ghuge, A. Torris and K. S. Nair, *ACS Appl. Polym. Mater.*, 2024, **6**, 11180–11192.

50 M. Nardi, L. Ceseracciu, V. Scribano, M. Contardi, A. Athanassiou and A. Zych, *Chem. Eng. J.*, 2024, **495**, 153400.

51 J. Kang, C. Wang, D. Li, G. He and H. Tan, *Phys. Chem. Chem. Phys.*, 2015, **17**, 16519–16524.

52 U. Panchal, M. L. Chaudhary, P. Patel, J. Patel and R. K. Gupta, *ACS Omega*, 2024, **9**, 10738–10747.

53 Y. Yan, J. Wu, Y. Wang, X. Fang, Z. Wang, G. Yang and Z. Hua, *ACS Sustain. Chem. Eng.*, 2021, **9**, 13695–13702.

54 C. C. Addis, R. S. Koh and M. B. Gordon, *Int. J. Adhes. Adhes.*, 2020, **102**, 102655.

55 F. Zhang, H. Li, T. Wang, X. Li, K. Li, J. T. Aladejana, D. Tian, J. Li and J. Li, *ACS Sustain. Chem. Eng.*, 2022, **10**, 17355–17368.

56 A. Del Prado, D. K. Hohl, S. Balog, L. M. De Espinosa and C. Weder, *ACS Appl. Polym. Mater.*, 2019, **1**, 1399–1409.

57 W. Liu, M. Wu, C. Ma, C. Liu, X. Zhang, Z. Wang and Z. Wang, *ACS Sustain. Chem. Eng.*, 2022, **10**, 13301–13309.